Applied Energy 239 (2019) 1037–1048

Contents lists available at ScienceDirect

Applied Energy

journal homepage: www.elsevier.com/locate/apenergy

Peer-to-peer-based integrated grid voltage support function for smart photovoltaic inverters

Hamada Almasalma*, Sander Claeys, Geert Deconinck

Departement Elektrotechniek, KU Leuven, Kasteelpark Arenberg 10, 3001 Leuven, Belgium
EnergyVille Research Center, Thor Park 8310, 3600 Genk, Belgium

HIGHLIGHTS

- Jacobi-proximal ADMM is applied to design peer-to-peer grid voltage support function.
- Push-sum gossip protocol is proposed as the underlying communication protocol.
- Linear voltage model is used to predict the voltage.
- The proposed algorithm is much faster than the Jacobi ADMM and the Dual Decomposition.
- The proposed algorithm succeeds in regulating the voltages within a reasonable time.

ARTICLE INFO

Keywords:
Smart inverter
Coordinated voltage control
Distributed control
Alternating Direction Method of Multipliers
Peer-to-peer

ABSTRACT

The increasing penetration of renewable energy sources is impacting the operation of the distribution grid. Whilst they are currently placing a burden on the distribution grid, it is generally agreed that these sources could also be used for active grid control, thereby contributing to a stable and secure grid. Smart photovoltaic inverters can contribute to active grid control, by expanding their features with added functions. In this paper, we develop a novel grid voltage support algorithm for smart photovoltaic inverters, based on distributed optimization and peer-to-peer communication. The Jacobi-Proximal Alternating Direction Method of Multipliers is applied in this paper to locally optimize reactive power compensation and active power curtailment of each inverter participating in the voltage control. We propose the use of a push-sum gossip protocol to enable peer-to-peer data interchange between inverters. We also use strategies to improve the robustness of the proposed algorithm: an acceleration strategy, a feedback strategy and an anti-windup strategy. A case study is presented, demonstrating the fast convergence of the algorithm and its ability to solve the voltage problems.

1. Introduction

Photovoltaic (PV) inverters were initially designed for low PV penetration levels. They were intentionally configured to inject as much active power as available from PV modules. PV inverters have been programmed to monitor the Point of Common Coupling (PCC) voltage and disconnect immediately after sensing the PCC voltage exceeding certain limits, to comply with the interconnection standards, such as IEEE 1547 and UL 1741 [1,2]. The earlier versions of the standards IEEE 1547 and UL 1741 prevent PV inverters from providing any type of grid support, and thus prohibit these inverters from actively participating in distribution system operation. This was not a problem when PV penetration levels were low.

High penetration of PV systems may create problems to maintain the voltage quality. Up till now, voltage quality in the distribution grid is achieved based on the layout of grid infrastructure that is capable of operating within limits even in worst case scenarios, with the assumption of unidirectional power flows. The planning of the infrastructure is quite straightforward: minimum and maximum load conditions are considered and minimum and maximum voltages in the grid are examined. The network is dimensioned in such a way that the minimum voltage is near the lower limit of the allowed voltage range and the maximum voltage is near the upper limit of the allowed voltage range. When connecting significant amounts of PV systems to the network, the assumption of unidirectional power flows is not always valid anymore and voltage profile of the network can be quite different than in the case without any generation. With maximum load conditions, PV generation increases the voltage level in the network and, hence, enhance the voltage quality in the grid. However, when the load on the

* Corresponding author.
E-mail address: hamada.almasalma@kuleuven.be (H. Almasalma).

https://doi.org/10.1016/j.apenergy.2019.01.249
Received 7 September 2018; Received in revised form 27 January 2019; Accepted 31 January 2019

Nomenclature

$[.]^{(k)}$	value at control iteration k
$[.]^{(t)}$	value at time step t
$[.]^{c}$	constant value
ΔP	change in active power P
ΔQ	change in reactive power Q
γ^{P}	curtailment acceleration factor
γ^{Q}	reactive acceleration factor
λ	Lagrangian multiplier
μ	power limit indicator
ρ	augmented penalty factor
τ	proximal penalization factor
c^{P}	penalty factor of active power
c^{Q}	penalty factor of reactive power
c_r	active power curtailment factor
k_G	gossiping iteration
S_d	inverter's kVA capacity
V	phase-to-neutral voltage
$V^{(k)}$	predicted voltage at iteration k
V^{meas}	actual-measured voltage
v^{P}	voltage sensitivity to the change in active power [V/kW]
v^{Q}	voltage sensitivity to the change in reactive power [V/kVAR]

network is at a minimum, the PV generation can reverse the power flows in the grid, what could lead to a rise of the voltage profile beyond its allowed limits [3].

The traditional solution to this problem is to reinforce the local distribution grid by installing more cables. However, generally this is quite expensive, as new infrastructure has to be installed. Another approach is by using the already installed infrastructure in a more optimal way, by coordination of the local generation, on load tap changers or other equipment used to control voltage in distribution networks. Voltage control techniques for distribution networks are reviewed in [4].

Smart PV inverters can contribute to active voltage control, by expanding their features with added grid voltage support functions (GVSFs) and without major hardware modifications. IEEE updated the connection Standard 1547 in 2014 [5], and UL 1741 was also updated to UL 1741 SA (Supplement A) [6]. The new standards identify inverter functions required for grid stability. These standards allow PV inverters to regulate the voltage through active power curtailment and reactive power compensation.

The control algorithm of the grid voltage support function (GVSF) can be designed mainly based on three strategies: communication-based centralized control, communication-less decentralized control, and communication-based distributed control [7]. A centralized control system uses a central optimizer to coordinate the GVSFs of the different inverters participating in the voltage control. It provides optimal coordination, taking into account the complete system behaviour. The central optimizer has access to all information about the inverters in its control area. Consequently, this centrally organized structure can coordinate the GVSFs based on exact information about local and global objectives [8]. However, centralized control of a large-scale distribution networks will reach the limits of scalability, computational complexity and communication overhead. Moreover, centralized control is a single point of failure. In [9], a centralized optimization-based voltage control system is implemented. The system controls voltage profiles of distribution grids, utilizing on-load tap changing (OLTC) transformers, PV inverters, and batteries. In [10], a coordinated voltage control of PVs and battery energy storage systems is discussed to address the voltage violation. Demand response is used in [11] to implement a real time centralized voltage control.

A decentralized communication-less voltage control system, on the other hand, mitigates the computational and communicational burden by using GVSFs with more advanced local processing capabilities. This system does not rely on any form of communication. Each GVSF is designed by ignoring the interactions from other GVSFs, the control decisions are based only on the available local information. In this case, optimal operation cannot be reached, as it is impossible to know the complete state of the distribution network and all operational boundary conditions of other inverters [12]. Different communication-less decentralized voltage control techniques are discussed in [13]. A hybrid voltage control system is implemented in [14], where both decentralized and centralized voltage control techniques are implemented to design a smart strategy for voltage ancillary service. To improve the performance of decentralized voltage control strategies, a centralized parameter tuning model is proposed in [15]. In the proposed model, voltage droop functions are formulated based on piecewise linearization.

In order to overcome the drawbacks of centralized and decentralized control, distributed control has been proposed in the literature. A comprehensive survey of distributed control algorithms for smart grids can be found in [16,17]. The distributed voltage control system is characterized by the complete absence of a central coordinator. In [18], a distributed coordinated voltage control algorithm is proposed. The algorithm uses a simplification method to deal with the lack of impedance and power information in distribution networks. Measurements of distribution phasor measurement units are used to transform networks with unknown impedance and power information to simplified networks with known equivalent parameters. A fully distributed voltage control based on multi-agent system is proposed in [19]. Peer agents coordinate to calculate voltage sensitivities by local and neighborhood measurements only.

Distributed voltage control can be formulated as a distributed optimization problem. Distributed optimization-based control algorithms have the potential to reach a (near) globally optimal solution under certain assumptions, thus achieving nearly the same control quality of centralized schemes. Distributed optimization-based voltage control algorithms appearing in the literature are mostly based on the Dual Decomposition method (DD) and the Alternating Direction Method of Multipliers (ADMM) [20]. DD and ADMM decompose a coupled optimization problem into sub-problems, suitable for distributed control. DD and ADMM apply the theory of Lagrangian multipliers and duality. ADMM also uses penalty function methods. Compared to DD, ADMM is numerically more stable and achieves faster convergence. As will be discussed later, the robustness and superior convergence properties of ADMM come from the use of additional penalty functions. Distributed voltage control algorithm based on DD is presented in [21]. The slow convergence of DD is analyzed experimentally in [22]. To overcome the drawbacks of DD, consensus ADMM is used in [23,24] to build a distributed voltage control system. Consensus ADMM is based on the distributed consensus protocol, where agents talk to each other to agree on the optimal change in their generation to maintain the voltages within limits. In consensus ADMM, each agent has local copies of the decision variables of its neighbours (auxiliary variables). The agent minimizes its sub-objective function over its own decision variables as well as over the decision variables of its neighbours.

It has been mentioned that centralized control systems often suffer from serious computation, robustness and communication issues for power systems with many controllable devices, distributed control is perhaps the only viable strategy for such systems. Nevertheless, these centralized control systems can achieve high performance. To achieve performance close to the performance of a centralized control system,

distributed voltage control systems rely on iterative algorithms. Hence, one of the main challenges in distributed voltage control is to reduce the number of iterations (as could as possible) to solve the voltage problem within a reasonable time, making the voltage profiles comply with the European standard EN 50160. To tackle this issue, our paper develops a novel fast distributed optimization-based voltage control algorithm. The algorithm uses a change in reactive power and active power curtailment of some participating PV inverters installed in the grid to regulate the voltage profiles within allowed limits. Our main contributions can be summarized as follows:

- We propose the use of the Jacobi-Proximal ADMM (JP-ADMM) for distributing a centralized voltage control problem. In JP-ADMM, the GVSFs are updated in parallel. Proximal penalization functions are used to preserve the convergence of the algorithm. Unlike in consensus ADMM, the agent in JP-ADMM does not need to agree on the decision variables of other agents, each agent treats the decision variables of other agents as constants and updates them in every control iteration.
- Secondly, we propose two factors for accelerating the convergence: one related to the reactive power compensation, and one related to the curtailment.
- Thirdly, we suggest the use of strategies to increase the performance of the proposed algorithm: feedback strategy, anti-windup strategy, and active/standby modes.
- Finally, we propose the use of a push-sum gossip protocol with JP-ADMM to enable peer-to-peer data interchange between the inverters.

The gossip-based JP-ADMM (G-JP-ADMM) algorithm can be integrated with the inner control loops of the PV inverter as shown in Fig. 1. To the best of our knowledge, this work is the first work proposing the use of G-JP-ADMM for designing a P2P-based GVSF.

The rest of this paper is organized as follows. To help the readers understand the linkage of the studied topic to the “big picture” of the P2P concept in energy systems, Section 2 discusses P2P-based integrated energy systems. The centralized optimization-based voltage control problem treated in this paper is formulated in Section 3. The proposed distributed algorithm for the GVSF (G-JP-ADMM) is presented in Section 4. The distributed network used in the case study and the parameters of the proposed algorithm are described in Section 5. Section 6 presents the simulation results. Finally, the paper is concluded in Section 7.

2. Towards a new energy paradigm for the distribution grid: P2P-based integrated energy systems

As photovoltaic systems and other renewable energy sources are typically highly distributed in the grid, operated by different owners and with different objectives, it is desirable that the management and control system of those energy systems operate in a fully distributed way as well. In this perspective, a P2P architecture seems to be a good method for controlling distributed energy resources (DERs) and enabling distributed energy trading [25].

This type of energy architecture, inspired by P2P computer networking, is characterized by the complete absence of a central management system. All local DERs (or agents), are equally important and can communicate to other agents, in a P2P fashion. In this architecture, there is a clear absence of a single point of failure. In the case a single agent fails, the other agents can still operate the grid in a stable way. Also when a single communication channel fails, the required information can still reach all necessary participants, via other agents. These properties make this architecture robust. Besides, information is kept local, reducing possible privacy concerns. On the other hand, all agents need a considerable amount of local intelligence, as they need to be able to execute the necessary optimizations.

It is impossible to impose this architecture on the whole distribution grid, as it incorporates thousands of DERs that are geographically very dispersed. To deal with this, breaking the complete grid down into smaller microgrids, containing only a limited amount of DERs, can be a solution. These microgrids operate then according to the P2P energy architecture.

The proposed scheme is shown in Fig. 2. The distribution grid is divided into several microgrids, hierarchically organized on different voltage levels. A microgrid can consist of a couple of low voltage feeders, physically connected to the same transformer, or a part of the medium voltage network on the same voltage level, for example. Each microgrid consists of several autonomous energy agents. On the connection points of two microgrids there is a coupling agent which serves as a gateway of one microgrid to the other microgrid. As the microgrids represented in this figure are separated by transformers or substations, these would be good candidates for such a coupling agent. Such a coupling agent represents the characteristics of the whole lower level microgrid (e.g. a low voltage feeder) on the higher level microgrid (e.g. a medium voltage network).

The proposed P2P-based energy architecture can be used to enable P2P energy trading. P2P energy trading concept provides local and regional energy producers with options to trade energy fairly within the neighborhood, within the community and within the vicinity of the distribution system. This will fundamentally change the current peer-to-grid paradigm where any surplus of local production can only be sold to transmission grids, and transform consumers position from energy/price takers to energy/price makers. P2P energy trading is discussed in details in [26–28]. Distributed management of energy flexibility and P2P balancing at the distribution level can be also designed based on the P2P-based energy architecture. In [29], a game theoretic approach for distributed energy management is developed, and blockchain method is applied to enable smart payment mechanisms.

This paper contributes to the P2P energy paradigm by developing a novel P2P-based grid voltage support function that can be integrated with the local control system of a PV inverter. The proposed approach allows to integrate P2P-based photovoltaic systems to carry out a distributed voltage control in each control zone of the proposed P2P energy architecture.

3. Problem formulation

A centralized optimization-based voltage control problem can be formulated as follows:

$$\underset{\Delta P, \Delta Q}{\text{minimize}} \quad \sum_{d \in \mathcal{D}} c_d^{\mathrm{P}} (\Delta P_d^{(t)})^2 + c_d^{\mathrm{Q}} (\Delta Q_d^{(t)})^2 \tag{1a}$$

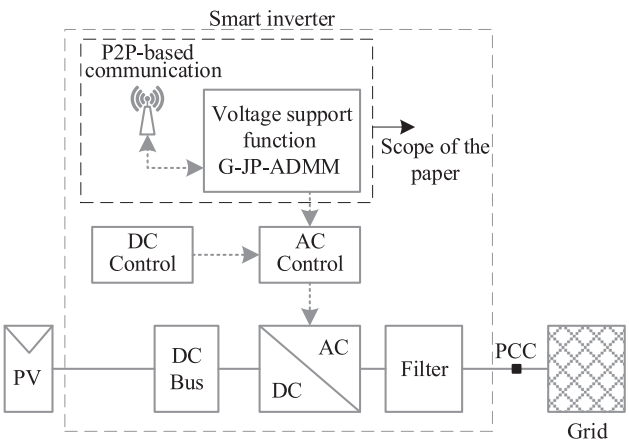

Fig. 1. General block diagram of smart PV inverter with P2P-based grid voltage support function.

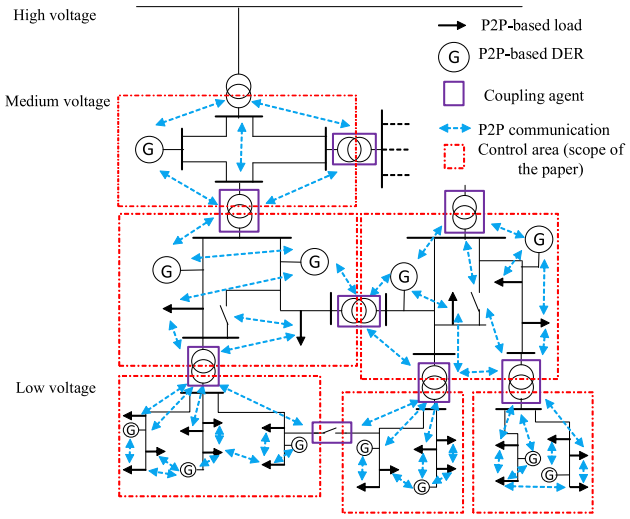

Fig. 2. P2P-based integrated energy systems.

subject to, $\forall\, d \in \mathcal{D}$

$$V^{\min} \leqslant V_d^{(t)} \leqslant V^{\max} \tag{1b}$$

$$f(V_d^{(t)}, \Delta P_i^{(t)}, \Delta Q_i^{(t)}) = 0, \quad \forall\, i \in \mathcal{D} \tag{1c}$$

$$(-c_r)(P_d^{\mathrm{PV}})^{(t)} \leqslant \Delta P_d^{(t)} \leqslant 0 \tag{1d}$$

$$-(\Delta Q_d^{\max})^{(t)} \leqslant \Delta Q_d^{(t)} \leqslant (\Delta Q_d^{\max})^{(t)} \tag{1e}$$

$$(\Delta Q_d^{\max})^{(t)} = \sqrt{(S_d)^2 - ((P_d^{\mathrm{PV}})^{(t)} + \Delta P_d^{(t)})^2} \tag{1f}$$

where $\mathcal{D}$ is the set of inverters participating in the voltage control. d, $t \in \mathbb{Z}^+$ are the number of inverters and of the time steps respectively. The objective function (1a) minimizes the total cost of all changes in active power P_d and reactive power Q_d needed to maintain the voltage within the limits $V^{\max}$ (maximum voltage limit) and $V^{\min}$ (minimum voltage limit). The total cost is the sum of the quadratic cost functions of the individual inverters: $c_d^{\mathrm{P}}(\Delta P_d^{(t)})^2$ represents the cost function of a change in active power of inverter d with an amount $\Delta P_d^{(t)}$, while $c_d^{\mathrm{Q}}(\Delta Q_d^{(t)})^2$ represents the cost function of a change in reactive power of inverter d with an amount $\Delta Q_d^{(t)}$. $\Delta P_d^{(t)}$ and $\Delta Q_d^{(t)}$ have to be within specified limits (1d)–(1f) to respect the maximum apparent power S_d and the maximum allowed curtailment. c_r is the curtailment factor that determines the curtailment percentage. $(P_d^{\mathrm{PV}})^{(t)}$ is the generation of the PV module connected to inverter d. $V_d^{(t)}$ in (1c) is the expected magnitude of the PCC voltage after applying $\Delta P_d^{(t)}$ and $\Delta Q_d^{(t)}$. The constraint (1c) represents the non-linear relation between $V_d^{(t)}$ and the active/reactive power injections of the inverters. The non-linear relation can be obtained from the AC power flow equations [30].

c_d^{P} and c_d^{Q} are constant factors used to prioritize the use of reactive power, while active power curtailment is performed only as a last resort. Therefore, c_d^{P} is set to be greater than c_d^{Q} in order to use most reactive power before starting to use active power curtailment [31].

A centralized controller solves the voltage control problem in three steps. First, at time step t, all input variables are gathered; these include PCC voltages and PV generation measured by the GVSFs. Secondly, the central optimizer solves the optimization problem (1a)–(1f) to optimally coordinate the inverters by minimizing the total change in reactive power compensation and active power curtailment. Finally, the controller sends the new set-points to the GVSFs. The major drawback of this approach is that a failure in the central coordinator completely disables the voltage control. Therefore, the next section presents a methodology that converts the centralized voltage control system into a distributed one.

It is worth to mention that network losses are not considered in the optimization problem. The proposed voltage control system can help in reducing the network losses, thanks to the curtailment of active power and local generation of reactive power. But indeed the voltage control system can increase the network losses. A constraint can be added to the optimization problem to limit network losses incurred by reactive power provision. Minimizing the network losses is out of scope of this paper.

4. Methodology

The objective function (1a) is basically a sum of separate cost functions, one for each inverter. The constraints (1d)–(1f) are local, meaning that they only constrain the local control variables ΔP_d and ΔQ_d, and therefore these constraints can be distributed easily. However, the cost functions cannot be distributed as they are coupled by the coupling constraint (1c). In this paper, multi-block ADMM is used to relax the coupling between the cost functions, to decompose the optimization problem (1a)–(1f) into sub-problems that can be solved in parallel.

The classic ADMM algorithm [32,33] is a 2-block system, it cannot be used to decompose the centralized optimization problem (1a)–(1f) into sub-problems that can be solved in parallel. The 2-block ADMM can be extended to: 1) multi-block Gauss-Seidel ADMM (GS-ADMM) and 2) multi-block Jacobi ADMM (J-ADMM). GS-ADMM is not amenable for parallelization as the blocks are updated one after another (sequentially). Additionally, the convergence is not guaranteed [34]. On the other hand, J-ADMM updates all the blocks in parallel. The convergence of J-ADMM can be guaranteed under certain assumptions [35], but it has a slow rate of convergence. Our simulation results show that the convergence of the J-ADMM algorithm is even slower than the convergence of the DD algorithm. In [36], a mathematical method called JP-ADMM is developed. The work of [36] shows that the 2-block ADMM can be extended to multi-block ADMM and preserve a convergence (at a rate of $o(1/k)$) by adding proximal terms to the augmented Lagrangian function. JP-ADMM is applied in this paper to solve the coupled centralized optimization problem by splitting it up into different sub-problems. These sub-problems are then solved separately by the GVSFs in parallel, imposing only the local constraints (1d)–(1f).

JP-ADMM applies an iterative optimization in a Jacobi-fashion of the Proximal Augmented Lagrangian Function (PALF), followed by a steep ascent update of the Lagrangian multipliers. In this paper, JP-ADMM is integrated with a push-sum gossip protocol to enable the GVSFs communicate with each other, and exchange their control variables and Lagrangian multipliers in a P2P fashion. With P2P communication, the GVSFs coordinate themselves and make the correct control decision in every particular situation to maintain the voltage within the required limits.

Since JP-ADMM is an iterative method, we define a control iteration $k \in \mathbb{Z}^{\geqslant 0}$ that moves the controlled voltage and the inverter control variables from $(V^{(k-1)}, P_d^{(k-1)}, Q_d^{(k-1)})$ to $(V^{(k-1)} + \Delta V^{(k)}, P_d^{(k-1)} + \Delta P_d^{(k)}, Q_d^{(k-1)} + \Delta Q_d^{(k)})$.

4.1. A constant linear voltage model

The use of the AC power flow model in (1c) results in a non-convex optimization problem that is difficult to handle in distributed optimization. To avoid the non-convexity, many works use linearised power flow equations [37,38]. Voltage sensitivities can be used to formulate a linear relation between controlled voltages and control variables ΔP_d and ΔQ_d. In Fig. 3, a simple distribution system is shown. The system consists of an inverter d connected to a bus d via a power line having a resistance R_{di} and a reactance X_{di}. Based on the distributed power flow equations of Baran and Wu [39], it can be shown that the voltage magnitude $V_i^{(k)}$ can be described by the following equation.

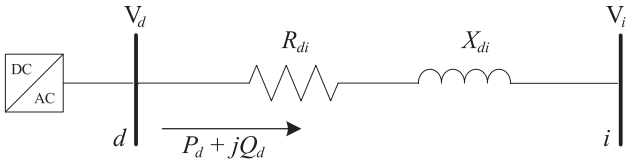

Fig. 3. A simple 2-bus distribution system.

$$V_i^{(k)} = \sqrt{(V_d^{(k)})^2 - 2(R_{di}P_d^{(k)} + X_{di}Q_d^{(k)}) + \frac{(R_{di}^2 + X_{di}^2)((P_d^{(k)})^2 + (Q_d^{(k)})^2)}{(V_d^{(k)})^2}} \tag{2}$$

For a small change $\Delta P_d^{(k)}$ and $\Delta Q_d^{(k)}$, a first order approximation can be used to simplify $V_i^{(k)}$ as follows:

$$V_i^{(k)} \approx (V_i^{\text{meas}})^{(k-1)} + \frac{\partial V_i}{\partial P_d}\Delta P_d^{(k)} + \frac{\partial V_i}{\partial Q_d}\Delta Q_d^{(k)} \tag{3}$$

where $(V_i^{\text{meas}})^{(k-1)}$ is the controlled voltage of bus i measured at the $(k-1)$-th iteration. As the partial derivatives are not constant and dependent on the system state, these are often approximated by [38]:

$$\frac{\partial V_i}{\partial P_d} \approx \frac{R_{di}}{V_{\text{nom}}} \quad \text{and} \quad \frac{\partial V_i}{\partial Q_d} \approx \frac{X_{di}}{V_{\text{nom}}} \tag{4}$$

where V_{nom} is the nominal voltage. Eq. (4) is a good approximation when the angle between the voltages at different nodes is small [8], which is the case in the distribution networks. For a set of inverters $\mathcal{D}$, Eq. (3) can be written as:

$$V_i^{(k)} \approx (V_i^{\text{meas}})^{(k-1)} + \sum_{d\in\mathcal{D}} v_{i,d}^{\text{P}}\,\Delta P_d^{(k)} + v_{i,d}^{\text{Q}}\,\Delta Q_d^{(k)} \tag{5}$$

where the coefficients $v_{i,d}^{\text{P}}$ and $v_{i,d}^{\text{Q}}$ are the approximated partial derivatives. These coefficients are considered as voltage sensitivity coefficients. $v_{i,d}^{\text{P}}$ and $v_{i,d}^{\text{Q}}$ represent the influence of active power and reactive power (respectively) of inverter d on the controlled voltage V_i. Eq. (5) represents a constant linear voltage model, since the voltage sensitivities are considered as constant coefficients. The voltage sensitivity coefficients can be calculated from the topology of the grid and the knowledge of the impedances of the lines. In [8,40], a direct load flow approach is presented. The approach is based on the calculation of two matrices named bus injection to branch current (BIBC) and branch current to bus voltage (BCBV). These matrices allow for easy calculation of the voltage sensitivity coefficients.

It is worth to mention that there are other methods that can be used to calculate (or estimate) the voltage sensitivities in distribution networks. If historical data of voltages, active power and reactive power are available, then linear regression can be used to estimate the voltage sensitivities, as detailed in [37]. The voltage sensitivities can be also estimated by applying small perturbations (small change in active and reactive power) into a given network, the voltage sensitivities are then determined by measuring the change in voltage.

The voltage sensitivity coefficients can be calculated before activating the voltage control system. The coefficients can be stored in the memory of each GVSF, and used by the proposed G-JP-ADMM algorithm to coordinate the inverters participated in the voltage control.

4.2. Equations of JP-ADMM algorithm

The main difference between the Augmented Lagrangian Function (considered in 2-block ADMM and multi-block J-ADMM) and the PALF (considered in JP-ADMM) is the addition of proximal penalty terms and acceleration factors for each sub-problem. As will be demonstrated later, these additions help to speed up the convergence of the algorithm. This subsection presents the derivation of the PALF, and how the PALF can be used to decompose the optimization problem (1a)–(1f) into sub-problems that can be solved in parallel. To derive the PALF, let's first define:

$$(U_d^{\max})^{(k)} = V_d^{(k)} - V^{\max}, \quad (U_d^{\min})^{(k)} = -V_d^{(k)} + V^{\min} \tag{6}$$

$$f_d^{(k)} = c_d^{\text{P}}(\Delta P_d^{(k)})^2 + c_d^{\text{Q}}(\Delta Q_d^{(k)})^2 \tag{7}$$

The PALF of the objective function (1a) and the coupled constraints (1b) and (1c) can be formulated as:

$$\begin{aligned}\mathcal{L}^{\text{PALF}}(\Delta P_d^{(k)}, \Delta Q_d^{(k)}, (\lambda_d^{\max})^{(k-1)}, (\lambda_d^{\min})^{(k-1)}) = \\ \sum_{d\in\mathcal{D}} (f_d^{(k)} + (\lambda_d^{\max})^{(k-1)}(U_d^{\max})^{(k)} \\ + (\lambda_d^{\min})^{(k-1)}(U_d^{\min})^{(k)} + \frac{\rho_d}{2}\max(0, (U_d^{\max})^{(k)})^2 \\ + \frac{\rho_d}{2}\max(0, (U_d^{\min})^{(k)})^2 + \frac{\tau_d}{2}(\Delta P_d^{(k)} - (\Delta P_d^{\text{c}})^{(k-1)})^2 \\ + \frac{\tau_d}{2}(\Delta Q_d^{(k)} - (\Delta Q_d^{\text{c}})^{(k-1)})^2\Big)\end{aligned} \tag{8}$$

where $(\lambda_d^{\max})^{(k-1)}$ and $(\lambda_d^{\min})^{(k-1)}$ are the Lagrangian multipliers associated with the d-th inequality constraint of (1b) and (1c). As will be shown later, these Lagrangian multipliers are calculated at the $(k-1)$-th iteration and considered in the minimization of the k-th iteration. Because of the Karush-Kuhn-Tucker (KKT) conditions, these multipliers cannot be negative. $\rho_d > 0$ is the augmented penalty factor. $\max(0, (U_d^{\max})^{(k)})^2$ and $\max(0, (U_d^{\min})^{(k)})^2$ are one-sided quadratic penalty functions used to penalize the objective function only when $V_d^{(k)}$ is higher than $V^{\max}$ or less than $V^{\min}$. $\tau_d > 0$ is the proximal penalization factor. $(\Delta P_d^{(k)} - (\Delta P_d^{\text{c}})^{(k-1)})^2$ and $(\Delta Q_d^{(k)} - (\Delta Q_d^{\text{c}})^{(k-1)})^2$ are the proximal terms. These terms penalize the deviation of the control variables at the k-th iteration ($\Delta P_d^{(k)}$ and $\Delta Q_d^{(k)}$) from the control variables $(\Delta P_d^{\text{c}})^{(k-1)}$ and $(\Delta Q_d^{\text{c}})^{(k-1)}$ that have been already calculated at the previous iteration (subscript c: constant). The proximal terms are used to preserve the convergence of the extended multi-block JP-ADMM algorithm. To derive the sub-problems, let's first define the following:

$$Y_{i,d}^{(k)} = v_{i,d}^{\text{P}}\,\Delta P_d^{(k)} + v_{i,d}^{\text{Q}}\,\Delta Q_d^{(k)} \tag{9}$$

$$C_{i,d}^{(k)} = \sum_{\substack{j\in\mathcal{D}\\ j\neq d}} (v_{i,j}^{\text{P}}\,\Delta(P_j^{\text{c}})^{(k-1)} + v_{i,j}^{\text{Q}}\,\Delta(Q_j^{\text{c}})^{(k-1)}) \tag{10}$$

To decompose the PALF into local Proximal Augmented Lagrangian Functions (PALFs), each GVSF fixes the control variables and Lagrangian multipliers of the other GVSFs by considering their control variables and Lagrangian multipliers that have been calculated at the previous $(k-1)$-th iteration. Based on this and based on Eq. (5), it can be shown that the local PALF of the GVSF d can be given by Eq. (11). The constants that do not affect the minimization of the local PALF are not included in (11).

$$\begin{aligned}\mathcal{L}_d^{\text{PALF}} = f_d^{(k)} + \sum_{i\in\mathcal{D}} \Big(((\lambda_i^{\max})^{(k-1)} - (\lambda_i^{\min})^{(k-1)})(Y_{i,d}^{(k)}) \\ + \frac{\rho_i}{2}\max(0, (V_d^{\text{meas}})^{(k-1)} + Y_{i,d}^{(k)} + C_{i,d}^{(k)} - V^{\max})^2 \\ + \frac{\rho_i}{2}\max(0, -(V_d^{\text{meas}})^{(k-1)} - Y_{i,d}^{(k)} - C_{i,d}^{(k)} + V^{\min})^2\Big) \\ + \frac{\tau_d}{2}(\Delta P_d^{(k)} - (\Delta P_d^{\text{c}})^{(k-1)})^2 + \frac{\tau_d}{2}(\Delta Q_d^{(k)} - (\Delta Q_d^{\text{c}})^{(k-1)})^2\end{aligned} \tag{11}$$

To reach the same solution as solving the optimization problem (1a)–(1f) with a constant linear voltage model, the JP-ADMM algorithm iterates as shown in Algorithm 1. The factor $\gamma_d > 0$ in the algorithm is the acceleration factor. $(V_d^{\text{meas}})^{(k)}$ is the PCC voltage of inverter d measured after applying $\Delta P_d^{(k)}$ and $\Delta Q_d^{(k)}$. At each iteration k of the JP-ADMM algorithm, the PALF is minimized by the GVSFs over $\{(\Delta P_1^{(k)}, \Delta Q_1^{(k)}), (\Delta P_2^{(k)}, \Delta Q_2^{(k)}), \ldots, (\Delta P_{|\mathcal{D}|}^{(k)}, \Delta Q_{|\mathcal{D}|}^{(k)})\}$ separately, in parallel, followed by an update of the Lagrangian multipliers. To guarantee the convergence, as demonstrated in [36], the proximal penalization factor should be as in (12), where $|\mathcal{D}|$ is the number of inverters with integrated GVSF.

$$\tau_d > \rho_d \left(\frac{|\mathcal{D}|}{2 - \gamma_d} - 1 \right) \tag{12}$$

Algorithm 1. JP-ADMM iterations

for $k = 0, 1, \ldots$ **do**

Update $\Delta P_d^{(k)}$ and $\Delta Q_d^{(k)}$ for $d = 1, \ldots, |\mathcal{D}|$ in parallel by:

$$\text{argmin}_{\{\Delta P_d^{(k)}, \Delta Q_d^{(k)}\}} \mathcal{L}_d^{\text{PALF}} \tag{13a}$$

Subject to the local constraints:

$$(-c_r)(P_d^{\text{PV}})^{(k-1)} \leqslant \Delta P_d^{(k)} \leqslant 0 \tag{13b}$$

$$-(\Delta Q_d^{\max})^{(k)} \leqslant \Delta Q_d^{(k)} \leqslant (\Delta Q_d^{\max})^{(k)} \tag{13c}$$

Update $(\lambda_d^{\max})^{(k)}$ and $(\lambda_d^{\min})^{(k)}$ for $d = 1, \ldots, |\mathcal{D}|$ in parallel by:

$$(\lambda_d^{\max})^{(k)} = \max(0, (\lambda_d^{\max})^{(k-1)} + \gamma_d \rho_d ((V_d^{\text{meas}})^{(k)} - V^{\max})) \tag{14a}$$

$$(\lambda_d^{\min})^{(k)} = \max(0, (\lambda_d^{\min})^{(k-1)} - \gamma_d \rho_d ((V_d^{\text{meas}})^{(k)} - V^{\min})) \tag{14b}$$

end for

4.3. Acceleration factor

The acceleration factor γ_d is used to have a steep ascent update of the Lagrangian multipliers, which helps in increasing the speed of convergence. In this paper, two acceleration factors are proposed: 1) the reactive acceleration factor γ_d^{Q} and 2) the curtailment acceleration factor γ_d^{P}. The acceleration factor γ_d^{Q} is used to accelerate the convergence of the controlled voltages to $V^{\max}$ (or $V^{\min}$) when reactive power compensation is used, whereas γ_d^{P} is used to accelerate the convergence when active power curtailment is used. As active power curtailment is penalized more than reactive power compensation, convergence of the controlled voltages to the accepted limits using curtailment is slower than the convergence when using reactive power compensation. Hence, γ_d^{P} should be greater than γ_d^{Q}.

4.4. Feedback strategy

There are two approaches regarding applying the control variables ΔP_d and ΔQ_d: 1) applying the control variables only after the control algorithm converges or 2) applying the control variables at each iteration. The latter is called Iterative Feedback Strategy (IFS). IFS has been used in [41] and is applied in this paper to improve the performance of the JP-ADMM algorithm. In IFS, at each iteration, the GVSF dynamically adjusts the inverter outputs, measures the PCC voltage $(V_d^{\text{meas}})^{(k)}$ and substitutes it in (14a) and (14b), to update the Lagrangian multipliers. IFS helps in increasing the voltage quality. Without IFS, the voltage during the convergence would stay beyond the accepted limits, without getting closer to these limits until the end of the iterations. Moreover, IFS helps in correcting the error of estimating the controlled voltage in (5). Additionally, if the generation and/or consumption changes during the computation, the GVSFs would implement outdated control variables.

4.5. Anti-windup strategy

The proposed control method continuously repeats two steps. First, the GVSFs optimize their compensation in parallel; exceeding the voltage limit has a fixed price, set by the Lagrangian multipliers. Secondly, the prices are updated; if one of the controlled voltages exceeds the voltage limit, then the corresponding price will be increased. This makes the over-voltage (or under-voltage) more expensive, and in the next iteration the GVSFs should decide to use more compensation to reduce the over-voltage. However, the optimization might be infeasible; there might not be enough compensation available to resolve the overvoltage issues. In such a case, the price will keep on increasing until the inverters saturate. Past this point, increasing the price further has no use and will slow down the response when the problem becomes feasible again. This effect is similar to 'windup' in classical control theory. The price updates are disabled when all inverters are saturated, which is referred to hereafter as the anti-windup strategy.

4.6. Active and standby modes

Active and standby modes are proposed in this paper to decide when to activate/deactivate the GVSFs. There is no need to operate the GVSFs continuously. When the controlled voltages are within the accepted limits, then there is no need to activate the GVSFs, whereas all the GVSFs should be activated when one (or more) of the controlled voltages is beyond the accepted limits. After activating the GVSFs, the Lagrangian multipliers can be used to know when to go to standby mode. The GVSFs can be deactivated when the Lagrangian multipliers of all the GVSFs return back to zero.

4.7. Push-sum gossip protocol

A communication layer is needed to disseminate the control variables and the Lagrangian multipliers among the GVSFs. Each GVSF needs these data to substitute them in Eqs. (13a)–(14b). This paper proposes the use of a P2P gossip-based push-sum algorithm presented in [42]. It is a fully distributed asynchronous communication protocol. It is scalable, fault-tolerant, resistant to packet losses and delays, and simple to implement. The algorithm is modified in this paper so that it can be used for dynamic disseminations. The modified algorithm is presented in Algorithm 2. It is an iterative algorithm with gossiping iteration k_G. Each GVSF tries to fill the matrix $\mathbf{S}_d^{(k_G)}$ before reaching the deadline. The deadline is used so that the GVSF does not need to wait forever when one of the GVSFs (or more) fails to communicate with the others. As shown in step 2 of the algorithm, the GVSF starts filling $\mathbf{S}_d^{(k_G)}$ by initializing the matrix with its own control variables, Lagrangian multipliers and power limit indicator $\mu_d^{(k)}$. The power limit indicator $\mu_d^{(k)}$ indicates whether the inverter reaches its power limits or not. The weight vector $\mathbf{W}_d^{(k_G)}$ is initialized to the unit vector $\mathbf{e}_d$, with 1 on the d-th position and 0 everywhere else.

Algorithm 2. Gossiping Push-Sum for JP-ADMM

1: Reset gossiping clock $\mathbf{T}_G$ and start it
2: **initialize:**
$k_G = 0$, $\sigma_d^{(k_G)} = 0$, $\mathbf{S}_d^{(k_G)} = \text{zeros}(|\mathcal{D}|, 6)$,
$\mathbf{W}_d^{(k_G)} = \mathbf{e}_d$, $(\mathbf{S}_d^{(k_G)})_{(d,:)} =$
$[\Delta P_d^{(k)}\ \Delta Q_d^{(k)}\ (\lambda_d^{\max})^{(k)}\ (\lambda_d^{\min})^{(k)}\ \mu_d^{(k)}\ \sigma_d]$
3: **while** $\sigma_d^{(k_G)}$ has zero entry (or entries) and $\mathbf{T}_G \neq$ deadline, **do**
4: $k_G \leftarrow k_G + 1$
5: Let $\{(\hat{\mathbf{S}}^{(r)}, \hat{\mathbf{W}}^{(r)})\}$ be all pairs sent to the GVSF d at the iteration $k_G - 1$
6: $\mathbf{S}_d^{(k_G)} \leftarrow \sum_r \hat{\mathbf{S}}^{(r)}$, $\mathbf{W}_d^{(k_G)} \leftarrow \sum_r \hat{\mathbf{W}}^{(r)}$
7: **if** all the entries of the vector $\mathbf{W}_d^{(k_G)}$ are non-zero, **then**
8: $\sigma_d^{(k_G)} = 1$
9: **end if**
10: Send $\frac{1}{2}\mathbf{S}_d^{(k_G)}$ and $\frac{1}{2}\mathbf{W}_d^{(k_G)}$ to a random other GVSF and to yourself
11: **end while**
12: $[\Delta \mathbf{P}_d^{(k)}\ \Delta \mathbf{Q}_d^{(k)}\ (\boldsymbol{\lambda}_d^{\max})^{(k)}\ (\boldsymbol{\lambda}_d^{\min})^{(k)}\ \boldsymbol{\mu}_d^{(k)}] = (\mathbf{S}_d^{(k_G)})_{(:,1:5)}/\mathbf{W}_d^{(k_G)}$

$\mathbf{S}_d^{(k_G)}$ consists of six vectors: $\Delta \mathbf{P}_d^{(k_G)}$, $\Delta \mathbf{Q}_d^{(k_G)}$, $(\boldsymbol{\lambda}_d^{\max})^{(k_G)}$, $(\boldsymbol{\lambda}_d^{\min})^{(k_G)}$, $\boldsymbol{\mu}_d^{(k_G)}$ and $\boldsymbol{\sigma}_d^{(k_G)}$. Each vector has $|\mathcal{D}|$ entries, each entry belongs to one of the GVSFs, e.g. the 5-th entry of $\boldsymbol{\lambda}_d^{\max}$ represents $\lambda_5^{\max}$ of the GVSF No. 5. As

will be discussed later, the vector $\boldsymbol{\mu}_d^{(k_G)}$ is used to detect the Lagrangian windup. In step 3 of the algorithm, the vector $\boldsymbol{\sigma}_d^{(k_G)}$ is used to make sure that the other GVSFs have filled their matrices before the GVSF stops the gossiping iterations of the control iteration k. In step 7, the GVSF detects a complete filling of its own $\mathbf{S}_d^{(k_G)}$ by observing the entries of the vector $\mathbf{W}_d^{(k_G)}$.

Each entry of $\mathbf{S}_d^{(k_G)}$ represents a sum and $\mathbf{W}_d^{(k_G)}$ is the weight of this sum (entries of the same row have the same weight). After stopping the gossiping iterations, the correct control variables and Lagrangian multipliers as well as the power limit indicators can be obtained by dividing each entry of the first five vectors by its own weight, as shown in step 12 (*e. g.* $\Delta P_5^{(k)} = (\Delta \mathbf{P}_d^{(k_G)})_{(5)}/(\mathbf{W}_d^{(k_G)})_{(5)}$ represents the active power curtailment of the GVSF No. 5 at iteration k). The matrix $\mathbf{S}_d^{(k_G)}$ and the vector $\mathbf{W}_d^{(k_G)}$ are always transmitted in pairs, so if a packet gets lost, all the other pairs continue to have the correct values.

4.8. The proposed G-JP-ADMM for P2P-based coordinated voltage control

In this subsection, we combine all the ideas and equations (presented in the previous subsections) in one algorithm. Algorithm 3 presents the proposed G-JP-ADMM algorithm. Algorithm 3 is proposed in this paper to bring smart functionalities to PV inverters by expanding their features with P2P-based GVSF to maintain the grid voltage within the accepted limits.

Algorithm 1 is extended here to include: acceleration for reactive power compensation, acceleration for active power curtailment, feedback strategy, anti-windup strategy, active mode and standby mode. These additional features improve the performance and the robustness of the algorithm. The Gossiping push-sum algorithm is used in Algorithm 3 to enable P2P data interchange between the GVSFs. In step 6, $\Delta \mathbf{P}_d^{(k)}$, $\Delta \mathbf{Q}_d^{(k)}$, $(\boldsymbol{\lambda}_d^{\max})^{(k)}$, $(\boldsymbol{\lambda}_d^{\min})^{(k)}$ and $\boldsymbol{\mu}_d^{(k)}$ are vectors with $|\mathcal{D}|$ entries, each entry represents a control variable, Lagrangian multiplier or power limit indicator for one of the GVSFs.

In step 13, the switching to the curtailment acceleration factor γ_d^P occurs when most of the available reactive power capacity are used (90%) and the active power curtailment has begun to be used (10%).

In step 18, the GVSF sets $\mu_d^{(k)} = 1$ when the inverter reaches its power limits. In case of voltage rise, $\mu_d^{(k)}$ is set to 1 when maximum reactive power absorption and maximum active power curtailment are used. In case of voltage drop, on the other hand, $\mu_d^{(k)}$ is set to 1 when maximum reactive power injection is used. Hence, a second comparison is used in step 17, to compare the injected reactive power with the upper limit. In step 20, when all inverters reach their power limits, each GVSF freezes its Lagrangian multipliers to avoid windup.

Algorithm 3. P2P-based GVSF

1: Each GVSF d carries out the following procedure:
2: $V_d^{\text{meas}} \leftarrow$ measure the PCC voltage
3: **if** $V_d^{\text{meas}} > V^{\max}$ (or $< V^{\min}$), or an active signal(s) is received, **then**
4: Send the received active signal(s) and your active signal using the standard push-sum gossip presented in [42]
5: Go to **active mode**
6: **initialize:**
$\Delta \mathbf{P}_d^{(0)} = \Delta \mathbf{Q}_d^{(0)} = (\boldsymbol{\lambda}_d^{\max})^{(0)} = (\boldsymbol{\lambda}_d^{\min})^{(0)} =$ zeros($|\mathcal{D}|$, 1)
$\mu_d^{(0)} = 0$, $(V_d^{\text{meas}})^{(0)} = V_d^{\text{meas}}$, $k = 1$
7: **begin** the control iterations:
8: $(P_d^{\text{PV}})^{(k-1)} \leftarrow$ measure the PV generation
9: Update $\Delta P_d^{(k)}$ and $\Delta Q_d^{(k)}$ based on (13a)–(13c)
10: Send $\Delta P_d^{(k)}$ and $\Delta Q_d^{(k)}$ to the AC control loop of the inverter
11: $(V_d^{\text{meas}})^{(k)} \leftarrow$ measure the PCC voltage (**feedback strategy**)
12: **if** $[\,|\Delta Q_d^{(k)}| > 0.9 \times (\Delta Q_d^{\max})^{(k)}\,]$ and $[\,\Delta P_d^{(k)} < 0.1\times - c_r (P_d^{\text{PV}})^{(k-1)}]$, **then**
13: $\gamma_d \leftarrow \gamma_d^{\text{P}}$ (**acceleration** of the curtailment)
14: **else**
15: $\gamma_d \leftarrow \gamma_d^{\text{Q}}$ (**acceleration** of the reactive power)
16: **end if**
17: **if** $\Delta Q_d^{(k)} = -(\Delta Q_d^{\max})^{(k)}$ and $\Delta P_d^{(k)} = -c_r (P_d^{\text{PV}})^{(k-1)}$, or $\Delta Q_d^{(k)} = \Delta (Q_d^{\max})^{(k)}$,
18: $\mu_d^{(k)} \leftarrow 1$ (**power limit indicator**)
19: **end if**
20: **if** all the entries of the vector $\boldsymbol{\mu}_d^{(k)}$ are 1, **then**
21: $(\boldsymbol{\lambda}_d^{\max})^{(k)} \leftarrow (\boldsymbol{\lambda}_d^{\max})^{(k-1)}$, $(\boldsymbol{\lambda}_d^{\min})^{(k)} \leftarrow (\boldsymbol{\lambda}_d^{\min})^{(k-1)}$ (**anti-windup**)
22: **else**
23: Update $(\boldsymbol{\lambda}_d^{\max})^{(k)}$ and $(\boldsymbol{\lambda}_d^{\min})^{(k)}$ based on (14a) and (14b)
24: **end if**
25: Execute Algorithm 2 to update the vectors $\Delta \mathbf{P}_d^{(k)}$, $\Delta \mathbf{Q}_d^{(k)}$, $(\boldsymbol{\lambda}_d^{\max})^{(k)}$, $(\boldsymbol{\lambda}_d^{\min})^{(k)}$ and $\boldsymbol{\mu}_d^{(k)}$
26: **if** all the entries of the vectors $(\boldsymbol{\lambda}_d^{\max})^{(k)}$ and $(\boldsymbol{\lambda}_d^{\min})^{(k)}$ are zero, **then**
27: Go to step 2 (**standby mode**)
28: **else**
29: $k \leftarrow k + 1$, repeat steps 8–29
30: **end if**
31: **end if**

5. Case study

The investigated case study network represents a typical Flemish (Belgium) semi-urban distribution network. This three-phase network operates with a nominal voltage of 230/400 V. It connects 62 households, as shown in Fig. 4. All main feeder cables are of type EAXVB 1 kV 4 × 150 mm^2 (impedance: 0.206 + j0.0778 Ω/km) except for the cable between node A and node B, which is of type EAXVB 1 kV 4 × 95 mm^2 (impedance: 0.320 + j0.0778 Ω/km). The cables connecting each household with the feeder are of type EXVB-Cu 1 kV 4 × 16 mm^2, with a fixed length of 30 m (impedance: 1.15 + j0.0828 Ω/km).

The active power consumption of the households is given by load profiles presented in [43]. The reactive power consumption is

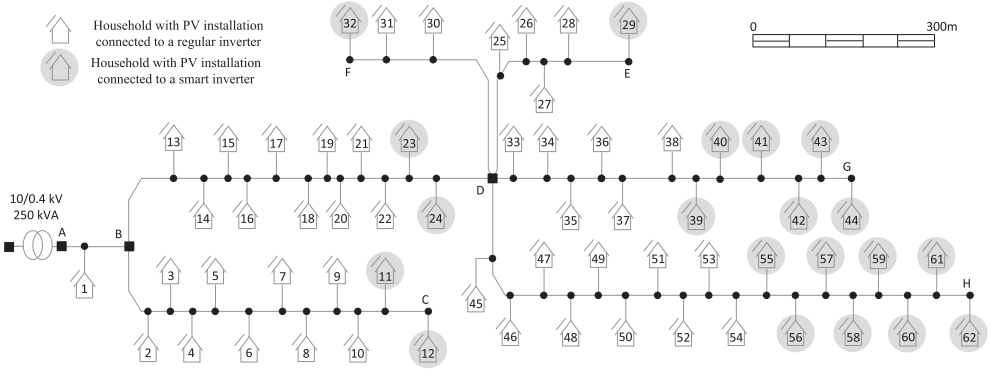

Fig. 4. Schematic diagram of the network used in the case study, all lengths are drawn to scale.

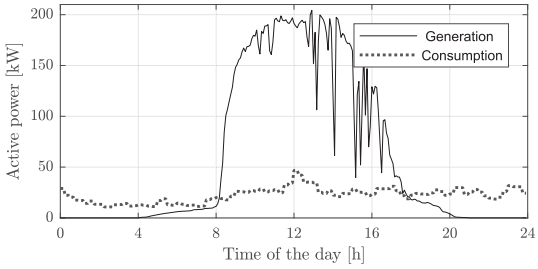

Fig. 5. Aggregated PV generation and active load profiles of the 62 households.

calculated by assuming a constant power factor of 0.85. Every household is equipped with a PV installation. The available generation of the PV installation is based on measured PV generation data from the rooftop PV installation at the department of electrical engineering (ESAT) of the KU Leuven. The inverters have different capacities ranging from 5 to 13 kVA. 20 of the PV inverters include the proposed P2P-based GVSF, which can curtail the active power output and regulate the reactive power generated by the smart inverters. The inverters at the end of the cables are selected in the case study to control the voltage, because they have higher impact on voltage variation than the inverters at the beginning of the feeder.

5.1. Simulation environment

The proposed algorithm is implemented in MATLAB R2018a and applied to the network of the case study to evaluate its performance. The MATPOWER package 6.0 for power flow analysis is used to calculate the measured voltages [44]. The CVX for solving convex optimization problems is used to solve the sub-optimization problem of each GVSF [45]. All of the numerical experiments are run on a workstation with an Intel Core i7-7700HQ CPUs (2.80 GHz) and 32 GB of RAM. In normal operation, each control iteration k is updated every 5 s. The push-sum gossip algorithm is executed with 100 ms communication latency, each GVSF sends the pair $(\frac{1}{2}\mathbf{S}_d^{(k_G)}, \frac{1}{2}\mathbf{W}_d^{(k_G)})$ to another random GVSF every 100 ms.

5.2. Case study parameters

To comply with the European standard EN 50160 on power quality [46], the voltage limits $V^{\max}$ and $V^{\min}$ are enforced to be ± 10% of the nominal phase voltage 230 V, resulting in $V^{\max} = 253$ V and $V^{\min} = 207$ V.

The curtailment factor c_r is set to 1, meaning that each inverter would curtail its whole active power, if needed.

To prioritize the use of reactive power, while active power curtailment is performed only as a last resort, the reactive power penalization factor c_d^{Q} is set to 1 and the curtailment penalization factor c_d^{P} is set to 200 (the tuning is based on trail and error). Active power curtailment can be penalized more to minimize its use, but having higher c_d^{P} would decrease the speed of convergence when the curtailment is used to return the voltages back to the limits. The penalty factors do not represent the actual unit cost of reactive power and active power curtailment (in euro). This is because minimizing the actual cost of operating the voltage control system is not the direct goal of the optimization problem (1a)–(1f). The goal of the optimization problem is to minimize the amount of reactive power and active power curtailment needed to maintain the voltages within the limits. If the minimum amount of reactive power and active power curtailment is used, then this will indirectly minimize the actual cost of operating the voltage control system. The objective function (1a) can be adapted to directly minimize the cost of operating the voltage control system. To this end, c_d^{P} can be set in such a way to represent loss of revenue from forgone energy due to active power curtailment, and c_d^{Q} can be set in such a way to represent reactive power unit cost considering inverter lifetime reduction and additional inverter losses, due to the reactive power provision [47,9].

To tune γ_d^{Q} and γ_d^{P}, we did two experiments. The first experiment was to tune γ_d^{Q}, whereas the second experiment was to tune γ_d^{P}. In the first experiment, we disabled the active power curtailment, to regulate the voltage profiles using only the reactive power. γ_d^{Q} was initialized to 1. After that, we increased γ_d^{Q} gradually till undesirable oscillation was noticed in the voltage profiles. In the second experiment, we disabled the reactive power compensation, to regulate the voltage profiles using only the active power curtailment. After that, we increased γ_d^{P} gradually till undesirable oscillation was noticed in the voltage profiles. For the case study of this paper, γ_d^{Q} is set to 500, whereas γ_d^{P} is set to 10^4.

The proximal penalization factor τ_d in (12) depends on the number of inverters $|\mathcal{D}|$ participating in the voltage control, the factor γ_d and the augmented penalization factor ρ_d. It is desirable to have small τ_d, to increase the speed of convergence by being less conservative in moving from one control variable to another, e.g. to have a bigger step from $\Delta Q_d^{(k-1)}$ to $\Delta Q_d^{(k)}$. In our work, we set $\tau_d = \rho_d\left(\frac{|\mathcal{D}|}{2-\gamma_d} - 1\right) + 1$ and ρ_d is set to be 0.001.

The sensitivity of the controlled voltages to the change in the active/reactive power were calculated based on the constant linear voltage model presented in Section 4.1.

The deadline for each GVSF to fill $\mathbf{S}_d^{(k_G)}$ is set to 1 min. For the 20 GVSFs, each GVSF needs around 10 gossiping iterations (see the convergence rate in [42]) to fill the matrices. With 100 ms latency, the GVSFs need around 1 s to fill the matrices. Hence, the time needed to fill the matrices is expected to be much less than 1 min.

6. Simulation results

The case study is executed for a low consumption summer day in July to be able to incorporate the effect of high PV generation. The simulation is performed for the entire day. Fig. 5 shows the total PV generation and the total active consumption of the 62 households.

6.1. Voltage rise mitigation

The low load and high PV generation result in reversed power flows. The reversed power flows cause a voltage rise beyond the EN 50160 limits. Fig. 6a shows the voltage profiles of the 62 households (phase to neutral voltages). One can see that most of the voltage profiles exceed the voltage limit $V^{\max} = 253$ V. To solve the voltage rise problem, the P2P-based GVSFs are activated. The regulated voltage profiles are shown in Fig. 6b. The existing violations of the over-voltage limit are mitigated. The voltage peaks, resulting from steep change in PV generation, fall beyond the limits, because the inverters need some time to react to the change.

To quantify the performance of the algorithm, a voltage quality metric E is proposed in this paper. The metric E, as illustrated in (15), integrates the over-voltages over time. This means that both the duration of the voltage rise problem and its severity will increase the metric E. A value of zero is the best possible value and indicates that there are no over-voltage issues. The higher the value of E, the worse the voltage problem. Fig. 7 shows the voltage quality metric E of the 62 households with and without voltage control. The voltage problem starts at household No. 19 and gets worse as we move towards the end of the feeder. One can notice that the voltage quality metric of the different households is reduced by a factor of 100 (approximately) after activating the GVSFs, which means that the voltage quality of the voltage profiles has been improved significantly.

$$E_d = \int_{t_{\mathrm{start}}=00:00}^{t_{\mathrm{end}}=24:00} (\max(V_d^{\mathrm{meas}} - V^{\max}, 0))dt \tag{15}$$

Fig. 8a shows the Lagrangian multipliers $\lambda_{62}^{\max}$[1] of smart inverter No. 62. The GVSF of inverter 62 is in standby mode between 00:00 and 08:40, when the voltages are within the limits. The GVSF starts to regulate the voltages at 08:40 (active mode), when the voltages start to violate the maximum limit. The GVSF returns back to standby mode

[1] $\lambda_{62}^{\min}$ is zero for the entire day, since there are no voltage drop issues.

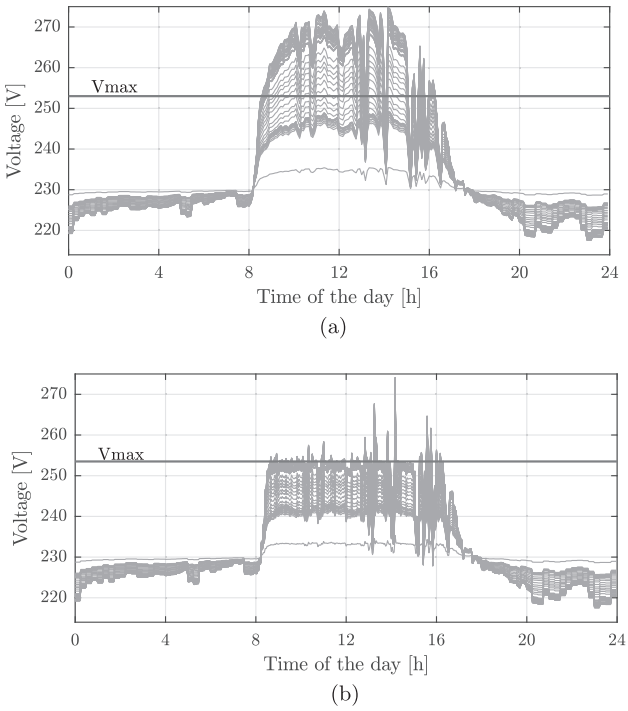

Fig. 6. (a) Voltage profiles without grid voltage support, (b) voltage profiles with grid voltage support.

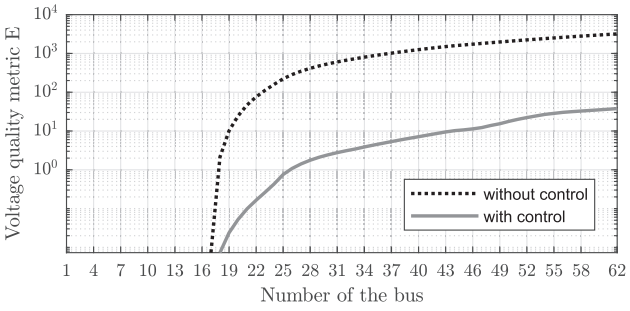

Fig. 7. Voltage quality metric E of the 62 households with and without grid voltage support.

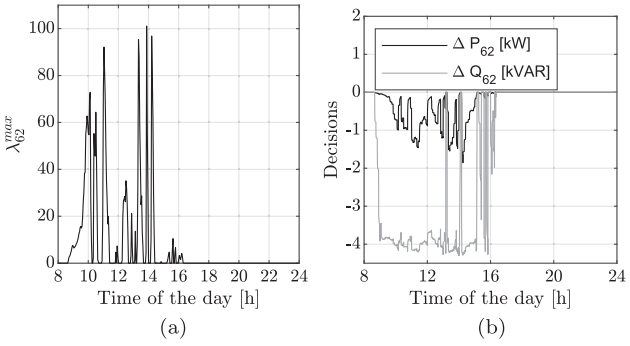

Fig. 8. (a) Lagrangian multiplier λ_{62}^{max} of smart inverter No. 62, (b) active power curtailment and reactive power compensation of smart inverter No. 62.

and the Lagrangian multiplier returns back to zero at 16:35, when the voltages return back to normal values due to solar irradiance reduction. Fig. 8b shows the control variables of smart inverter No. 62. The average reactive power inverter 62 absorbs during the day is around −4 kVAR, whereas the average active power the inverter curtails is around −0.5 kW. ΔP_{62} and ΔQ_{62} return to zero when the Lagrangian multipliers return back to zero.

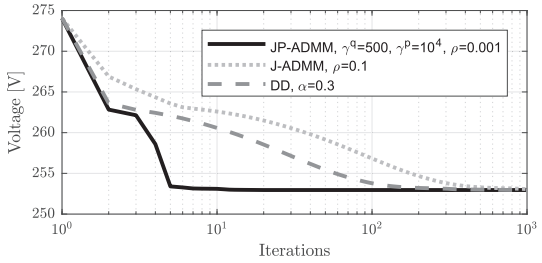

Fig. 9. Comparison of the convergence speed between JP-ADMM, J-ADMM and DD.

6.2. The convergence of JP-ADMM, J-ADMM and DD

Fig. 9 shows a comparison of the speed of convergence of the proposed G-JP-ADMM algorithm (Algorithm 3), the J-ADMM algorithm and the dual decomposition-based voltage control algorithm presented in [21]. The J-ADMM algorithm can be implemented as presented in Algorithm 3, but without including the proximal terms and the acceleration factor γ_d [36]. As discussed earlier, the best results for the G-JP-ADMM algorithm (in terms of convergence speed) occur when $\gamma^Q = 500$, $\gamma^P = 10^4$, and $\rho = 0.001$ (for all the GVSFs). For the case study of this paper, the best results for the J-ADMM algorithm occur when ρ is set to 0.1 for all the GVSFs. The J-ADMM algorithm does not converge when ρ is higher than 0.1. The fastest convergence of the DD algorithm presented in [21] is achieved when the step size α is set to 0.3 for all the GVSFs. The DD algorithm diverges when α is higher than 0.3.

The three algorithms are implemented at each smart inverter and are executed at 14:00, the time when the voltage profiles have the highest voltage rise. Fig. 9 presents the convergence of the PCC voltage of smart inverter No. 62 (worst voltage). We can see that the G-JP-ADMM algorithm is clearly the fastest one among the compared algorithms. The G-JP-ADMM algorithm returns the PCC voltage back to the limit in less than 10 iterations, whereas the J-ADMM algorithm needs around 500 iterations and the DD algorithm needs around 370 iterations to bring the PCC voltage back to the limit. From this study, we can also conclude that the J-ADMM algorithm is even slower than the DD algorithm. It is worth to mention again that G-JP-ADMM enjoys a fast preserved convergence thanks to the proposed acceleration factors and the applied proximal penalization functions.

6.3. Accuracy of the linear voltage model

The linear voltage model presented in Section 4.1 is used to predict the voltage of iteration k before applying the control decisions $\Delta P_d^{(k)}$ and $\Delta Q_d^{(k)}$. The optimization of the control decisions depends highly on how accurate the prediction is. The prediction made by Eq. (3) is quite accurate. Fig. 10 shows a comparison between the predicted voltage and the actual one of smart inverter No. 62 (62-bus network). The algorithm is executed for two hours, from 14:00 till 16:00 (period of worst voltage problem). The predicted voltage is calculated by Eq. (3), whereas the measured voltage is calculated by exact power flow equations (using MATPOWER). One can notice the high accuracy of the linear voltage model. The maximum error is around 0.3%.

The high accuracy of the prediction is due to two reasons; first, the algorithm of the proposed method is an iterative one. The system takes small steps towards the final solution. At each iteration, the change in reactive power and active power curtailment is small. For a small change, the first order approximation of Eq. (2) is quite accurate, and second, thanks to the feedback strategy of the proposed G-JP-ADMM method, the system corrects the error in its decision at each control iteration. This means that the error does not accumulate. Fig. 11 presents a comparison between the predicted voltage and actual voltage for two cases, with and without feedback strategy. With feedback strategy the error is around 0.3%, whereas without feedback the error is around 1.2%. One can notice that without feedback strategy the algorithm brings the actual voltage to

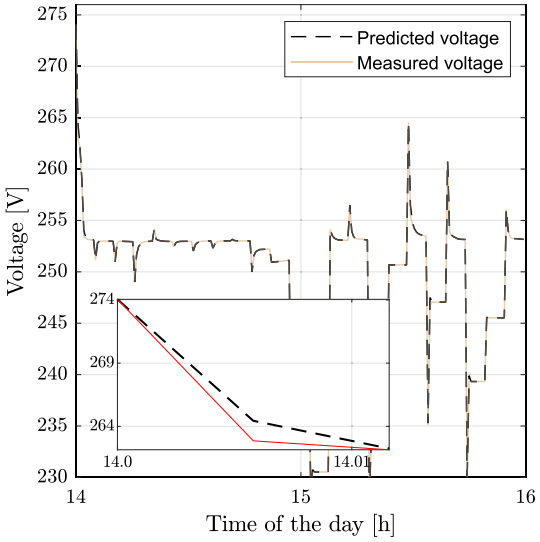

Fig. 10. Predicted voltage vs. actual voltage of smart inverter No. 62.

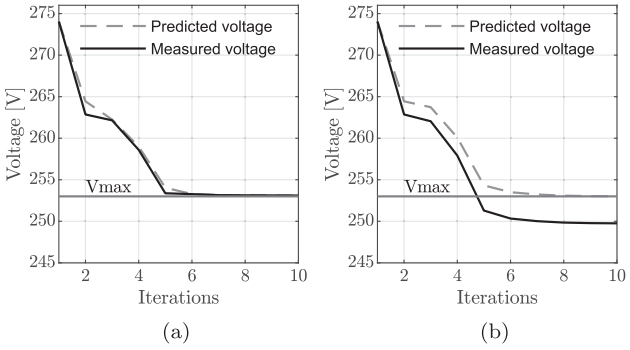

Fig. 11. (a) Voltage regulation with feedback strategy, (b) voltage regulation without feedback strategy.

a value lower than the maximum limit. This means that the voltage is over-regulated, and the amount of absorbed reactive power and curtailed active power is more than needed.

6.4. 124-bus case study

To test the performance of the proposed algorithm on a large system, we have extended the network of the case study from 62-bus (with 20 smart inverters and 42 regular inverters) to 124-bus (with 50 smart inverters and 74 regular inverters). We extended the following feeders to host more households: feeder DE to host 25 households, feeder DG to host 32 households, and feeder DH to host 40 households. Additionally, we set the size of the 124 inverters to 5 kVA. Fig. 12a shows the voltage profiles of the 124 households without voltage control, whereas Fig. 12b shows the voltage profiles with voltage control. Again we notice that our proposed method succeeds in improving the quality of the voltage profiles significantly.

Fig. 13a demonstrates the scalability of the proposed method. It shows a comparison between voltage convergence of smart inverter No. 62 (62-bus network) and voltage convergence of smart inverter No. 124 (124-bus network), at 14:00. In case of 20 agents (62-bus network), the algorithm takes 8 iterations to bring the voltage back to the limit, whereas the algorithm takes 15 iterations to bring the voltage back to the limit in case of 50 agents (124-bus network). Hence, increasing the number of agents does not lead to exponential increase in the number of iterations. This is because in G-JP-ADMM, each agent treats the decision variables of other agents as constant.

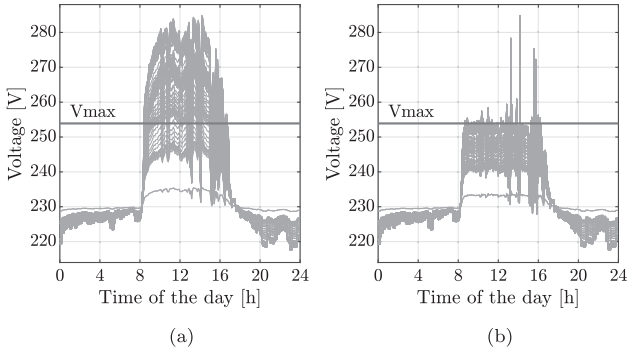

Fig. 12. (a) Voltage profiles of 124-bus network without voltage control, (b) voltage profiles of 124-bus network with voltage control.

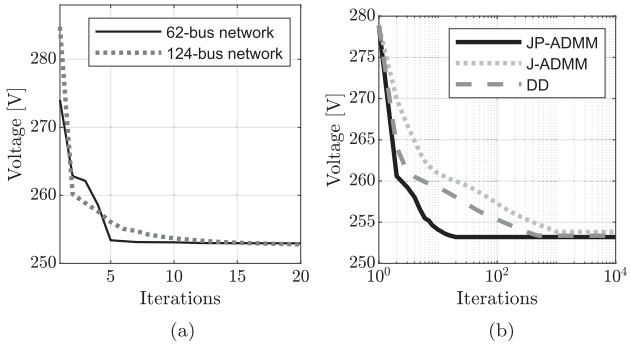

Fig. 13. (a) Voltage convergence of smart inverter No. 62 (62-bus network) and smart inverter No. 124 (124-bus network), (b) 124-bus network: comparison of the convergence speed between JP-ADMM, J-ADMM and DD.

Fig. 13b shows a comparison between JP-ADMM, DD and J-ADMM, at 14:00 (124-bus network). The figure presents the convergence of PCC voltage of smart inverter No. 124. Again we notice that our proposed method is much faster than DD and J-ADMM.

6.5. Scalability of the push-sum gossip protocol

Fig. 14 shows the number of GVSFs each GVSF needs to communicate with to know the control decisions and the Lagrangian multipliers of each GVSF in the system. In case of 20 smart inverters, each GVSF needs to communicate with 8–13 GVSFs. In case of 50 smart inverters, each GVSF needs to communicate with 10–14 GVSFs. The number (of GVSFs to be communicated with) is not fixed since each agent contacts random agents at each control iteration. The results of Fig. 14 demonstrate the fact that each GVSF needs to communicate with some GVSFs (not all) to know the status of all other GVSFs. The results also demonstrate the scalability of the proposed push-sum gossip protocol. The gossip-based protocol enjoys exponential rapid spread of information. Increasing the number of smart inverters does not significantly increase the burden of communication.

6.6. Discussion

The time needed to finish one control iteration of G-JP-ADMM, J-ADMM and DD is around 5 s.[2] Based on the results presented in the 62-bus case study, the proposed G-JP-ADMM needs around 0.67 min

[2] Based on the performance of the workstation, and assuming the following: (a) 1 s as the time needed to measure the PV generation and the voltage, (b) 50 ms as the response time of the AC control loop, (c) 100 ms communication latency.

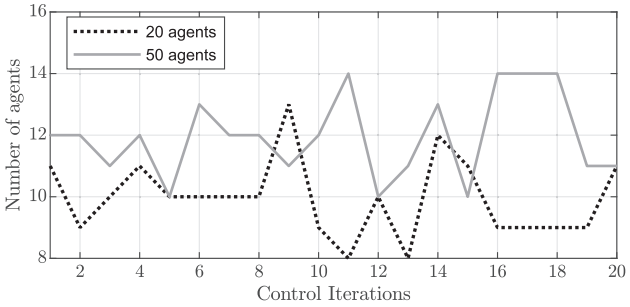

Fig. 14. Number of agents to be communicated with per control iteration.

(5 s× 8 iterations) to bring the voltage of bus No. 62 to the accepted limit (124-bus case study: 1.25 min), whereas J-ADMM needs around 41.7 min (5 s× 500 iterations) and DD needs around 30.8 min (5 s× 370 iterations). We can conclude from this analysis that the proposed algorithm succeeds in regulating the voltage profiles to comply with the European standard EN 50160, whereas DD and J-ADMM fails to comply with the standard EN 50160, since they fail to maintain all 10 min rms voltages within the range $[V_{\text{nom}} - 10\% = 207\,\text{V}, V_{\text{nom}} + 10\% = 253\,\text{V}]$.

7. Conclusion

This paper presents a novel voltage control algorithm for photovoltaic inverters to expand their features with added grid voltage support function. To eliminate the problems that a centralized control method possesses, having a single point of failure, the grid voltage support function is designed based on a distributed control method. The Jacobi-Proximal Alternating Direction Method of Multipliers is used to convert a centralized optimization-based voltage control system into a distributed one. All local grid voltage support functions communicate with the other grid voltage support functions in a peer-to-peer fashion. A push-sum gossip algorithm is used for the dissemination of the variables of each grid voltage support function to all grid voltage support functions. The grid voltage support functions can then act according to the received information, in cooperation with each other. Each grid voltage support function locally computes the reactive power compensation and active power curtailment of its inverter by considering the variables of the other grid voltage support functions as constants.

To speed up the convergence of the proposed algorithm, reactive/curtailment acceleration factors are proposed. An anti-windup strategy is also proposed to have faster convergence in case of Lagrangian windup. A feedback strategy is used to improve the quality of the voltage profiles. To prevent operating the grid voltage support functions all the time, active and standby modes are proposed. We have shown that our algorithm can achieve fast convergence and is able to mitigate the voltage rise problem of distribution networks with high penetration of photovoltaic systems.

Acknowledgements

This research is supported by an SB PhD fellowship from FWO-Vlaanderen.

References

[1] Basso T. IEEE 1547 and 2030 standards for distributed energy resources interconnection and interoperability with the electricity grid. No. NREL/TP-5D00-63157. National Renewable Energy Lab.(NREL), Golden, CO (United States); 2014.
[2] UL Standards, UL 1741 standard for inverters, converters, controllers and interconnection system equipment for use with distributed energy resources, second edition; 2010. https://standardscatalog.ul.com/standards/en/standard_1741_2.
[3] Barth B, Concas G, Zane EB, Franz O, Frías P, Hermes R, et al., PV Grid-Final Project Report, Horizon 2020: PV GRID Project.
[4] Xu T, Taylor P. Voltage control techniques for electrical distribution networks including distributed generation. IFAC Proc Vol 2008;41(2):11967–71.
[5] IEEE Standard for Interconnecting Distributed Resources with Electric Power Systems - Amendment 1. IEEE Std 1547a-2014 (Amendment to IEEE Std 1547-2003); 2014. p. 1–16.
[6] Gonzalez S, Johnson J, Reno MJ, Zgonena T. Small commercial inverter laboratory evaluations of UL 1741 SA grid-support function response times. 2016 IEEE 43rd photovoltaic specialists conference (PVSC). IEEE; 2016. p. 1790–5.
[7] Almasalma H, Engels J, Deconinck G. Peer-to-peer control of microgrids. In: 8th IEEE Benelux PELS/PES/IAS young researchers symposium; 2016. p. 1–6.
[8] Zad BB, Lobry J, Vallée F. A centralized approach for voltage control of MV distribution systems using DGs power control and a direct sensitivity analysis method. 2016 IEEE international energy conference (ENERGYCON). IEEE; 2016. p. 1–6.
[9] Efkarpidis N, De Rybel T, Driesen J. Optimization control scheme utilizing small-scale distributed generators and oltc distribution transformers. Sustain Energy, Grids Networks 2016;8:74–84.
[10] Kabir M, Mishra Y, Ledwich G, Xu Z, Bansal R. Improving voltage profile of residential distribution systems using rooftop PVs and battery energy storage systems. Appl Energy 2014;134:290–300.
[11] Zakariazadeh A, Homaee O, Jadid S, Siano P. A new approach for real time voltage control using demand response in an automated distribution system. Appl Energy 2014;117:157–66.
[12] De Brabandere K, Bolsens B, Van den Keybus J, Woyte A, Driesen J, Belmans R. A voltage and frequency droop control method for parallel inverters. IEEE Trans Power Electron 2007;22(4):1107–15.
[13] Demirok E, Gonzalez PC, Frederiksen KH, Sera D, Rodriguez P, Teodorescu R. Local reactive power control methods for overvoltage prevention of distributed solar inverters in low-voltage grids. IEEE J Photovolt 2011;1(2):174–82.
[14] Calderaro V, Galdi V, Lamberti F, Piccolo A. A smart strategy for voltage control ancillary service in distribution networks. IEEE Trans Power Syst 2015;30(1):494–502.
[15] Ji H, Wang C, Li P, Zhao J, Song G, Ding F, et al. A centralized-based method to determine the local voltage control strategies of distributed generator operation in active distribution networks. Appl Energy 2018;228:2024–36.
[16] Molzahn DK, Dörfler F, Sandberg H, Low SH, Chakrabarti S, Baldick R, et al. A survey of distributed optimization and control algorithms for electric power systems. IEEE Trans Smart Grid 2017;8(6):2941–62.
[17] Antoniadou-Plytaria KE, Kouveliotis-Lysikatos IN, Georgilakis PS, Hatziargyriou ND. Distributed and decentralized voltage control of smart distribution networks: models, methods, and future research. IEEE Trans Smart Grid 2017;8(6):2999–3008.
[18] Wang X, Wang C, Xu T, Meng H, Li P, Yu L. Distributed voltage control for active distribution networks based on distribution phasor measurement units. Appl Energy 2018;229:804–13.
[19] Wang X, Wang C, Xu T, Guo L, Li P, Yu L, et al. Optimal voltage regulation for distribution networks with multi-microgrids. Appl Energy 2018;210:1027–36.
[20] Boyd S, Parikh N, Chu E, Peleato B, Eckstein J. Distributed optimization and statistical learning via the alternating direction method of multipliers. Found Trends Mach Learn 2011;3(1):1–122.
[21] Almasalma H, Engels J, Deconinck G. Dual-decomposition-based peer-to-peer voltage control for distribution networks. CIRED - Open Access Proc J 2017 2017(1):1718–21.
[22] Almasalma H, Claeys S, Mikhaylov K, Haapola J, Pouttu A, Deconinck G. Experimental validation of peer-to-peer distributed voltage control system. Energies 2018 2018;11(5):1–22.
[23] Liu HJ, Shi W, Zhu H. Distributed voltage control in distribution networks: Online and robust implementations. IEEE Trans Smart Grid 2018;9(6):6106–17.
[24] Šulc P, Backhaus S, Chertkov M. Optimal distributed control of reactive power via the alternating direction method of multipliers. IEEE Trans Energy Convers 2014;29(4):968–77.
[25] Giotitsas C, Pazaitis A, Kostakis V. A peer-to-peer approach to energy production. Technol Soc 2015;42:28–38.
[26] Zhang C, Wu J, Zhou Y, Cheng M, Long C. Peer-to-peer energy trading in a microgrid. Appl Energy 2018;220:1–12.
[27] Lüth A, Zepter JM, del Granado PC, Egging R. Local electricity market designs for peer-to-peer trading: the role of battery flexibility. Appl Energy 2018;229:1233–43.
[28] Zhou Y, Wu J, Long C. Evaluation of peer-to-peer energy sharing mechanisms based on a multiagent simulation framework. Appl Energy 2018;222:993–1022.
[29] Noor S, Yang W, Guo M, van Dam KH, Wang X. Energy demand side management within micro-grid networks enhanced by blockchain. Appl Energy 2018;228:1385–98.
[30] Das D, Kothari D, Kalam A. Simple and efficient method for load flow solution of radial distribution networks. Int J Electr Power Energy Syst 1995;17(5):335–46.
[31] Olivier F, Aristidou P, Ernst D, Van Cutsem T. Active management of low-voltage networks for mitigating overvoltages due to photovoltaic units. IEEE Trans Smart Grid 2016;7(2):926–36.
[32] Glowinski R, Marroco A. Sur l'approximation, par éléments finis d'ordre un, et la résolution, par pénalisation-dualité d'une classe de problèmes de dirichlet non linéaires. Revue française d'automatique, informatique, recherche opérationnelle. Analyse numérique 1975;9(R2):41–76.
[33] Gabay D, Mercier B. A dual algorithm for the solution of nonlinear variational problems via finite element approximation. Comput Math Appl 1976;1(2):17–40.
[34] Chen C, He B, Ye Y, Yuan X. The direct extension of ADMM for multi-block convex minimization problems is not necessarily convergent. Math Program 2016;155(1–2):57–79.
[35] He B, Hou L, Yuan X. On full jacobian decomposition of the augmented Lagrangian method for separable convex programming. SIAM J Optim 2015;25(4):2274–312.

[36] Deng W, Lai M-J, Peng Z, Yin W. Parallel multi-block ADMM with o(1/k) convergence. J Sci Comput 2017;71(2):712–36.
[37] Weckx S, D'Hulst R, Driesen J. Voltage sensitivity analysis of a laboratory distribution grid with incomplete data. IEEE Trans Smart Grid 2015;6(3):1271–80.
[38] Brenna M, De Berardinis E, Carpini LD, Foiadelli F, Paulon P, Petroni P, et al. Automatic distributed voltage control algorithm in smart grids applications. IEEE Trans Smart Grid 2013;4(2):877–85.
[39] Baran ME, Wu FF. Optimal capacitor placement on radial distribution systems. IEEE Trans Power Deliv 1989;4(1):725–34.
[40] Díaz G, Gómez-Aleixandre J, Coto J. Direct backward/forward sweep algorithm for solving load power flows in ac droop-regulated microgrids. IEEE Trans Smart Grid 2016;7(5):2208–17.
[41] Dall'Anese E, Dhople SV, Giannakis GB. Photovoltaic inverter controllers seeking AC optimal power flow solutions. IEEE Trans Power Syst 2016;31(4):2809–23.
[42] Kempe D, Dobra A, Gehrke J. Gossip-based computation of aggregate information. 44th Annual IEEE symposium on foundations of computer science, 2003. Proceedings. IEEE; 2003. p. 482–91.
[43] Labeeuw W, Deconinck G. Residential electrical load model based on mixture model clustering and Markov models. IEEE Trans Ind Inform 2013;9(3):1561–9.
[44] Zimmerman RD, Murillo-Sánchez CE. Matpower 6.0 Users Manual; 2016.
[45] Grant MC, Boyd SP. The CVX Users Guide, Release 2.1. http://cvxr.com/cvx/doc/CVX.pdf.
[46] Masetti C. Revision of European standard EN 50160 on power quality: Reasons and solutions, 14th IEEE international conference on harmonics and quality of power (ICHQP); 2010, 1–7.
[47] Gandhi O, Rodríguez-Gallegos CD, Gorla NBY, Bieri M, Reindl T, Srinivasan D. Reactive power cost from PV inverters considering inverter lifetime assessment. IEEE Trans Sustain Energy 2018;1(1). 1–1.